Additive Manufacturing of Bioceramic Scaffolds for Bone Tissue Regeneration with Emphasis on Stereolithographic Processing

Additive manufacturing of bioceramic scaffolds for bone tissue regeneration, with emphasis on stereolithographic processing

Francesco Baino*, Elisa Fiume, Giulia Magnaterra, Enrica Verné

Institute of Materials Physics and Engineering, Applied Science and Technology Department, Politecnico di Torino, Corso Duca degli Abruzzi 24, 10129 Torino, Italy

* Corresponding author: F. Baino
Tel.: +39 011 090 4668
Fax: +39 011 090 4624
E-mail: francesco.baino@polito.it

Abstract

Advanced bone tissue engineering approaches rely on implanting synthetic grafts for the management of mid to large bone defects in order to overcome the common limitations associated to the use of transplant materials. Bioceramics are especially effective due to their versatile functional properties and processing methods. This chapter provides a picture of ceramic scaffolds for bone tissue engineering, focusing on additive manufacturing technologies and, specifically, the emerging method of digital light processing. The functional and structural complexity of natural bone makes the design of scaffolds a complex challenge as their chemical, structural and functional properties have to meet very specific requirements, e.g. adequate support properties, bone-bonding capability and a macro- and microporous structure to promote cell colonization and vascularization. Many fabrication techniques are currently available for the production of porous artificial biomaterials. Among them, the class of additive manufacturing technologies is one of the most promising for the development of mechanically competent and structurally highly-defined scaffolds with tailored properties for bone tissue engineering applications.

Keywords: Bioceramics; Scaffold; Additive manufacturing; Porosity; Digital light processing.

1. Scaffolds for bone repair: an overview

The scaffold, also known as tissue template and/or artificial extracellular matrix, is a 3D porous structure that acts as a biocompatible implantable substrate [1] on which cells can attach, proliferate and differentiate in order to synthetize new bone tissue until the complete filling of the original bone defect in achieved [1],[2].

Andrés Segovia, a Spanish classical guitarist, proposed a fascinating definition of the role of scaffolds using these words [3]: *"When one puts up a building, he makes an elaborate scaffold to get everything into its proper place. But when one takes the scaffold down, the building must stand by itself with no trace of the means by which it was erected. That is how a musician should work"*.
Table 1 summarizes the main functions that should be performed by a scaffold intended for tissue engineering applications.

Table 1. Functions of biomedical scaffolds (adapted from [4])**.**

Primary Functions of Scaffold
Substrate for cell adhesion
Delivery vehicle for exogenous cell, growth factors and genes
Temporary mechanical support for new tissue growth
Barrier to the infiltration of surrounding tissue that may hinder the process of regeneration
Maintenance of the shape of the defect by avoiding distortion

Given the complex and deeply interlocked nature of a biological system, scaffolds have to satisfy multiple requirements at the same time, as depicted in Figure 1 [5].

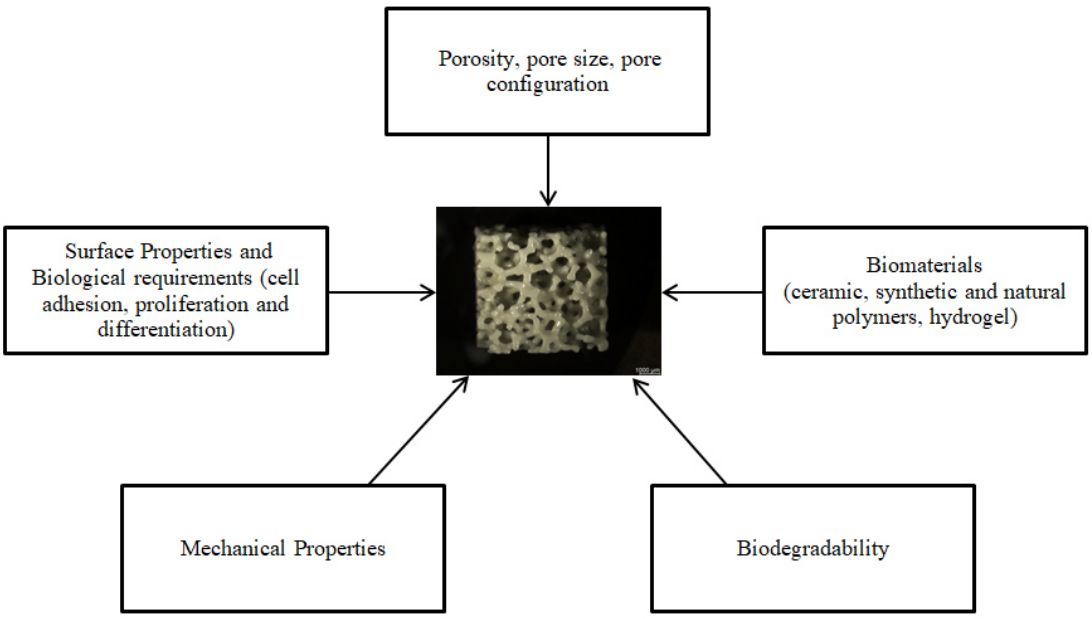

Figure 1. Key factors involved in the design of scaffolds for bone tissue engineering.

Osteoconductivity, controlled biodegradability and biocompatibility [6] are essential features to be considered in the design of tissue-engineered scaffolds intended for bone defect repair, where new

tissue growth and scaffold resorption are concurrent events leading to the replacement of the implanted biomaterials by newly formed bone. Highly biocompatible materials have to be used in order to avoid persistent inflammatory response and cytotoxicity within the body [3]. In addition, scaffolds should have suitable structural properties to provide proper mechanical support over the whole healing process [6]. Scaffolds should also exhibit sufficient biological affinities to promote the integration with host tissue, growth of relevant cells [2] and regeneration of healthy tissue [7] as well as have suitable porosity features, which are necessary to allow cell migration, diffusion of nutrients and vascularization [3].

Ideally, the structural parameters of scaffolds (e.g. total porosity, pore size, shape etc.) should be designed according to the implant site following a similarity criterion; in fact, bone tissue exhibits different structural properties depending on the anatomical position in the skeletal system. Therefore, if surgery on spongy bone is required, highly porous scaffolds are preferable; on the other hand, if the problem concerns the cortical bone, mechanically strong scaffolds with low porosity and oriented strut will be required [7].

2. Scaffold requirements

Tissue-engineering scaffolds are designed to fulfil a series of requirements that are summarized in Table 2, along with their effects.

Table 2. Characteristics of the scaffold and their desirable effects.

Scaffold requirements	**Desirable features**
Biocompatibility	• Non-toxic degradation products • Non-inflammatory scaffold components, avoiding immune rejection
Biodegradability	• Controlled scaffold degradation which can complement tissue ingrowth while maintaining sufficient mechanical integrity • Degradable by host enzymatic or biological processes • Allows invading host cells to produce their own extracellular matrix
Bioactivity	• Beneficial interaction between scaffold material and host tissue: formation of a stable bond • Osteoconductive and osteoinductive properties • Inclusion of biological cues and growth factors to stimulate cell attachment, proliferation and differentiation
Scaffold architecture	• Interconnected pores allowing diffusion and cell migration • Microporosity, which provides large surface area for improved cell-scaffold interactions • Macroporosity to allow cell migration and invasion of vasculature • Sufficient porosity to facilitate cell ingrowth without weakening mechanical properties • Tailored pore size and distribution to target tissue and cells

	• Inbuilt vascular channels to enhance angiogenesis *in vivo*
Mechanical Properties	• Compressive, elastic and fatigue strength comparable to host bone, favouring cell mechanoregulation pathways and maintenance of structural integrity *in vivo* • Scaffold material that can be readily manipulated by clinicians to treat individual patient's bone defects

2.1 Biocompatibility

This is the first criterion that every tissue-engineered scaffold should fulfil [6]. As regards scaffolds, the term biocompatibility was defined as "*the capability of a material to facilitate natural cellular and molecular activity within a scaffold in the absence of systemic toxicity*" [8]. Therefore, biocompatible scaffolds allow cells to adhere, migrate and proliferate on their surface without the risk of triggering any dangerous inflammatory responses [6], and/or potentially toxic effects, both locally and systemically [9]. Good biocompatibility also promotes osteoconductivity, osteoblast proliferation and osteoinductivity [8].
In order for the scaffold to be biocompatible, it is necessary to carefully select the material with which it is manufactured. Suitable materials for bone tissue engineering applications should firmly bond to the natural bone *in situ* and stimulate new tissue growth and regeneration [9].
It has been shown that calcium phosphate and bioactive glass scaffolds are highly biocompatible and, furthermore, actively improve the tissue repair process through releasing calcium, phosphate and silicate ions that play a role in accelerating osteogenesis [8]. Methods for assessing the biocompatibility of scaffolds can be found in specific international standards [10].

2.2 Porosity

Pore size and porosity percentage of the scaffolds are key parameters to achieve physiological development of newly formed tissue [11]. An ideal scaffold for cancellous bone repair should have an open-cell porous architecture, with porosity > 50-60 vol.% [2], where more than 60% of the pores should have a size between 100-400 μm and at least 20% is expected to have a size below 20 μm [3]. Porosity percentage and pore size directly affect the osteoinductive and osteoconductive capabilities of the scaffold [12]. In principle, scaffolds with analogous total pore volume and pore size can also be considered suitable for the repair of cortical bone provided that the mechanical properties are adequate (e.g. compressive strength >100 MPa vs. 2-12 MPa of cancellous bone, see section 2.3).
A suitable porosity range, above 50-60 vol.% of interconnected macropores, confers to the scaffold adequate mass transport properties for cell migration, attachment and interaction with the biological environment [6], as well as the passage of nutrients and bioactive molecules. Moreover, it has been demonstrated that suitable porosity features can improve vascularization and spatial organization between cell growth and extracellular matrix (ECM) production, thus leading to a considerable enhancement of the biomineralization process [8]. Large pores (size around 200-300 μm) lead to direct

osteogenic pathways [2],[9]. The prevailing opinion in the literature is that the pore size should be between 200-400 µm in order to allow greater cell migration and proliferation, and the consequent formation of new tissue [13].
On the contrary, smaller pores (<100 µm) were found to be beneficial for chondrogenesis [14]. Too small pores may lead to poor vascularisation [11] and limited cell migration, causing the formation of cell capsules around the edges of the scaffold [9].
In general, it is necessary for the pores not to be too large, as this would excessively decrease the mechanical resistance of the final product [9], [6].
The ideal degree of porosity should be found so as to allow sufficiently high permeability and interconnectivity for nutrient supply and waste removal as well as adequate stiffness and resistance to the loads transmitted from the healthy bone adjacent to the scaffold [2].
Interconnectivity (Figure 2) is a key requirement to ensure the transport of nutrients and the elimination of waste products [15]. An in vivo study with hydroxyapatite scaffolds showed that low pore interconnection enables limited tissue penetration and chondral tissue formation but does not guarantee proper bone tissue growth [15].
The shape of the pores can also influence the mechanical of the scaffold [6]. Gong et al. performed fatigue tests (cyclic stress-strain) on scaffolds with triangular and circular pores with a total porosity of about 60 vol.% and found that scaffolds with circular pores are more resistant than those with triangular pores [6].

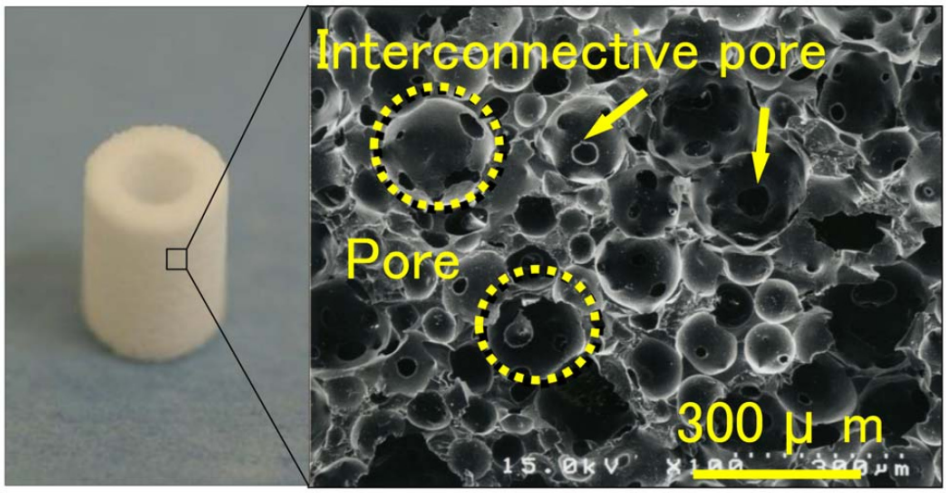

Figure 2. Pores and interconnectivity of pores showed in hydroxyapatite scaffold. Image reproduced from Doi et al. [16] under the terms of the Creative Commons Attribution Licence.

2.3 Mechanical properties

In order to be functional, a scaffolds should have biomechanical properties comparable to those of the host healthy bone [12],[8]. It has to maintain a certain mechanical integrity over the whole duration of the treatment, in order to support the physiological healing process until the newly formed tissue has

become able to physically support itself [8]. It should have a Young's module similar to that of natural bone in order to avoid stress shielding phenomena and favour early tissue regeneration [17]. Strong scaffolds can be obtained by building anisotropic structures with oriented pores [9]. For example, in order to replace cortical bone a good scaffold should have a compressive strength ~130-180 MPa and Young's modulus ~ 12-18 GPa.

Pore size, interconnectivity and architecture directly impact on the mechanical properties of porous implants [15]. For example, studies on hydroxyapatite scaffolds have shown that decreasing the pore size yields higher compressive strength [15].

The compressive strength is the most common and easy-to-determine mechanical parameter for brittle ceramic scaffolds [18]. In accordance with ASTM F2883-11, the compressive strength of implantable ceramic scaffolds should be assessed following the ASTM C1424 that is valid for advanced ceramics [18].

In addition, it has been proven that the mechanical properties of the scaffold affect the mechanotransduction properties of the bone cells attached to its surface; in other words, mechanical stimuli from the biomaterial (e.g. stiffness) can be converted in different biochemical responses by cells and, thus, different bone regeneration rates and extent. In fact, there also seems to be a correlation between mechanotransduction and the potential osteoinductive properties of the scaffold [12]. Not all anchorage-dependent cells respond similarly to scaffold stiffness [11]: endothelial cells, for example, migrate and proliferate more easily on more rigid substrates [11].

2.4 Biodegradability

As the tissue regenerates, the scaffold should ideally degrade in a controlled manner over time [8]. This property is not mandatory (for example, hydroxyapatite scaffolds are permanent implants) but is desirable in many cases.

The biodegradability of the scaffold is dependent on the type of material and its clinical application: β-TCP-based scaffolds show a bioresorption rate similar to that of new bone formation, whereas hydroxyapatite scaffolds are generally characterized by better chemical durability [8].

Biomaterials degradation is influenced by the presence of enzymes or macrophages in the physiological fluids [7].

The rate of scaffold degradation may change depending on the different geometry and pore-strut architecture adopted. It is therefore necessary to test different production methods to find the optimal one according to the needs [8]. Scaffold degradation can be investigated following the standard ISO 10993-14 [18].

2.5 Surface properties and interaction with cells

The scaffold needs to be made in complex and even irregular shapes. The scaffold should serve as a model for natural bone growth and should therefore mimic the hierarchical structure of natural bone. With regard to cortical bone, for example, its internal architecture should be similar to the small vascular channels, Volkmann's channels and the gaps in the osteocytes and Haversian channels [9].

As already mentioned, the scaffold needs to be carefully designed in order to ensure a highly-interconnected porous structure [9].
Several studies have shown that the characteristics of the scaffold surface affect the amount, type and conformation of proteins and cells that will adhere to it [9]. A rough surface may improve cell adhesion, but excess roughness must be avoided, otherwise the cells may fail to develop focal adhesion plaques [4]. This is a general trend but providing an "ideal" range of "optimal" roughness for cell adhesion and proliferation is impossible, as the behaviour of each specific cell type is concurrently influenced by type of material and shape of nano-/micro-features on the surface (e.g. grooves, pits, islands).
The performance of a scaffold is strongly affected by the interaction between the material surface and the surrounding biological environment and is often mediated by proteins absorption by the biological fluid [19]. Chemistry, roughness and surface topography strongly influence the protein layer on which the formation of surface bonds directly aimed at binding only certain types of cells depends. Proteins create a specific interface through which cells can respond to scaffold's topographical cues determined by the macrostructure, and the chemical features of the surface are responsible for the cells attachment to the structure [19]. Surfaces with nanometric topography increase the availability of proteins and amino acids by promoting cell adhesion to a large extent [19].
Some examples in the literature suggest the incorporation of growth factors into scaffolds because they can improve and speed up the growth of new bone [14]. In fact, bone morphogenetic proteins (BMPs) help the development of osseous tissue and can trigger the differentiation and proliferation of osteoprogenitor cells. Vascular endothelial growth factor (VEGF) has often been used because it can improve blood vessel formation [14].

3. Conventional methods for ceramic scaffold fabrication

Scaffold manufacturing techniques could be divided into two main groups: conventional methods and non-conventional methods, which correspond to additive manufacturing technologies [9].
Scaffolds can be made using conventional techniques such as freeze-drying, gas foaming, sponge replication, solvent casting and particulate leaching, sol-gel-foaming method, phase separation (TIPS, DIPS, RIPS) [13], melt, dry, wet-spinning and electro-spinning [1]. In general, conventional techniques include all those techniques that are not based on a CAD/CAM design and are relatively easy and cheap to apply [9]. However, these methods have several limitations, including poor reproducibility [1][13], and the inability to obtain a precise and reliable control on the internal porosity, geometry and interconnectivity of the 3D structure [6]. From the biological point of view, the latter could be a severe drawback as a random and uncontrolled 3D porous network could determine an heterogeneous distribution of cells, causing uneven tissue growth [20]. The most common conventional manufacturing technique are summarized in Table 3 and described in the following sections.

3.1 Foaming methods

These techniques rely on the use of a foaming agent to produce air bubbles that are responsible for the formation of the porosity at the macroscale. After preparing a colloidal suspension (or slurry), pores are

created due to the action of a porogen by either injecting the gas directly or generating gas as product of a chemical reaction, thermal decomposition or addition of surfactants [9].
Foaming methods include techniques such as gel-cast foaming, H_2O_2 foaming and sol-gel foaming. However, all these techniques do not assure the high pore interconnectivity required for successful bone implants and do not guarantee a scaffold with good mechanical properties [9]. In this regard, Chen et al. fabricated highly porous 45S5 Bioglass® foams by including a surfactant in the sol that, after vigorous agitation, yielded a bone-like porous structure but the resulting scaffolds were highly brittle [21].

3.2 Phase separation methods

These techniques have been originally developed to obtain polymeric scaffolds and are usually divided in three groups depending on the main parameters that cause demixing of the solution [22]; for example, temperature-induced phase separation (TIPS) is based on the change of the temperature causing separation between polymer (optionally embedding ceramic or glass inclusions) and solvent [22]. As regards diffusion-induced phase separation (DIPS), addition of a vapour or a liquid (i.e. a non-solvent) is necessary; reaction-induced phase separation (RIPS) is based on a chemical reaction leading to the phase separation in the original polymeric solution; precipitation induced by a change in pH is also included in this class [22].
TIPS is used to obtain both polymeric and polymer-matrix composite scaffolds embedding porous ceramic (glass) micro-/nanoparticles to increase bioactivity and mechanical strength/stiffness [9].
TIPS is based on the solubility-temperature dependence existing between two different polymers: two polymers may be soluble in each other at a given temperature but completely insoluble at a lower temperature. Therefore, if a solution of these polymers is made and then the solution is cooled down to the critical temperature of the solution, they will separate, forming two different phases, one less rich in polymer and one richer in polymer. The less polymer-rich phase will be removed and the porous structure will be finally obtained [9].
TIPS is used to obtain porous scaffold with pore diameter from 1 to 100 μm and porosity over 95 vol.%. For example, Szustakiewicz et al., obtained porous scaffold based on synthetic hydroxyapatite and poly(L-lactide) (PLLA) using TIPS supported by salt leaching process [23].
Maquet et al. built a scaffold of bioresorbable polymers (poly-(D,L-lactide) (PDLLA) and poly(lactide-co-glycolide) (PLGA)) and 45S5 Bioglass®. They constructed two different sets of samples by varying the amount of glass powder; in both cases, they obtained a porosity greater than 90 vol.% and overall good bioactivity imparted by the glass inclusions [24].
Degli Esposti et al. created bioresorbable and bioactive porous scaffold based on poly(3-hydroxybutyrate) (PHB) and hydroxyapatite particles that were able to sustain the growth and proliferation of MC3T3-E1 cells, had suitable porosity for bone repair and exhibited good bioactivity due to the presence of hydroxyapatite [25].

3.3 Spinning methods

These techniques allow obtaining nano- or micrometric fibres, which are useful especially for the regeneration of nerves, and are divided into dry, wet, melt spinning methods and electrospinning [22].
Melt-spinning technique uses a melted polymer that is extruded through a die with the desired section, while dry spinning and wet spinning use concentrated solutions that are similarly extruded through a die of proper section. For both methods, removal of the solvent is necessary to obtain the fibres.
Electrospinning can use both polymer solutions in volatile solvent (electrospinning solution) and polymeric melts (melt electrospinning). It is a versatile technique that allows making continuous fibres from submicrometric to nanometric diameters [22].
An interesting study reported the production of 45S5 Bioglass® scaffolds with biodegradable nanofibrous coatings obtained with electro-spinning. The composite scaffold obtained by combining bioactive glass and electrospun polymeric nanofibers (PCL-PEO, P(3HB), PHBV) allowed the formation of a layer of bone-like nanostructured hydroxyapatite upon immersion in physiological fluids and the possibility of achieving controlled drug release [26].
Hong et al. fabricated hierarchal nanoporous bioactive glass fiber mats by using electrospinning technique and P123-PEO as co-templates for the nanopores. As a result, multiscale porosity was obtained with the mesoporous glass fibres arranged into 3D macroporous mats. These hierarchical scaffolds were proposed for potential application in bone tissue engineering combined with drug delivery [27].

3.4 Thermal consolidation of particles

The methods that are part of this group are characterized by the use of sacrificial particles added to the green body that will be sintered. These particles will form pores upon thermal degradation and they are typically polymers or of synthetic (e.g. polyethylene) or natural origin (e.g. rice husk or starch) [9]. These techniques are relatively inexpensive but usually they do not allow obtaining highly porous scaffolds with good interconnectivity among pores [9]**.**

3.5 Sponge replica method

This method relies on the use of porous templates of natural material (e.g. marine sponge) or synthetic material (e.g. polyurethane sponge) that are immersed in a ceramic (glass) slurry [28] to create sintered positive replicas of the sponges with a high level of porosity and bone-like 3D architecture [9]. The sponge is the organic phase of the scaffolds and only serves as a template for the inorganic phase, since it will be completely removed during the production process [9]. In fact, the ceramic (glass)-coated porous organic template will have to undergo a double heat treatment, the first to eliminate the organic phase and the second to consolidate the ceramic (glass) particle by sintering [9]. As a result, a porous ceramic structure is obtained showing the same architecture of the sacrificial template [28].
This method allows obtaining scaffolds with structures very similar to the trabecular architecture of natural cancellous bone and high levels of porosity (about 90 vol.%), but often these scaffolds have poor mechanical properties [9]. Usually, foam replication is applied to fabricate porous glass, glass-ceramic, biphasic calcium phosphate and hydroxyapatite scaffolds [29]. A limitation of this technique is the poor capability to create a solid network with high density and strong mechanical properties [29].

In 2006, Chen et al. used polyurethane commercial foams as a sacrificial template to be dipped in a slurry of commercial 45S5 Bioglass® containing PVA as a binder. This was one of the first scaffold batches that were successfully obtained by this method: these samples had a very high porosity (85-90 vol.%) and interconnected and open macropores between 510-720 μm, which make them very similar to spongy bone but, at the same time, too weak to be used for bone repair (compressive strength between 0.1-0.4 MPa) [30].
Tripathi et al. used this method to build hydroxyapatite scaffolds with interconnected oval pores (diameter 100-300 μm and wall thickness ~50 μm). The homogeneous distribution of pores and the pore wall thickness provided large surface area to promote protein attachment and cell proliferation [31].
Fu et al. fabricated foam-replicated 13-93 glass scaffolds with total porosity of 85 vol.% and pore size of 100–500 μm. In this case, the scaffolds exhibited significantly higher compressive strength (11 MPa) as compared to other examples produced by the same method in the literature due to the good sinterability of the material, yielding to well-densified ad strong struts. In addition, 13-93 glass scaffolds successfully supported the proliferation of MC3T3-E1 pre-osteoblastic cells [29].
Wu et al. tried to improve the mechanical properties of mesoporous bioactive glass scaffolds obtained via sponge replica method by depositing a silk coating on their struts; in spite of a certain improvement, the scaffold strength obtained from compressive tests still remained low (< 0.3 MPa).

Table 3. Conventional methods vs. non-conventional methods.

Conventional methods	**Non-conventional methods**
- Inability to obtain a scaffold with a precise architecture and controlled porosity - Inadequate to create patient-specific scaffolds - Techniques strongly dependent operators - Usually fast and not too expensive techniques	- Fabrication complex internal 3D structures and patient-specific geometries - Possibility to use heterogeneous materials - Industrial scalability - Sometimes limited choice of materials - High cost of the process
METHODS: Solvent casting and particulate leaching Gas foaming Freeze-drying Sol-gel Melt, dry, wet-spinning and electrospinning Phase separation (TIPS, DIPS, RIPS) Sponge replication method	METHODS: Select laser sintering (SLS) Stereolithography (SLA) Fused deposition modelling (FDM) Laminated object manufacturing (LOM) Solid ground curing 2-photon polymerization Robocasting Ink-jet printing

	3D printing (3DP) 3D fibre deposition

4. Additive manufacturing technologies for ceramic scaffold fabrication

Despite the improvements that have been made over the last years, conventional techniques are still strongly dependent on the process rather than the design and exhibit some inherent limitations that make it impossible to finely control the architecture of the scaffolds [4].
In order to overcome these drawbacks, since the second half of the 1980s [34] many researchers have been developing a number of additive manufacturing technologies as a valid alternative to obtain detailed and extensive control on the fabrication process [4], [35].
Over the last two decades, with the development of rapid prototyping techniques, a great number of tissue-engineered scaffolds have been created for potential use in clinical practice using new materials and ground-breaking technologies [6]. These methods make it now possible to create customized scaffolds for a targeted tissue regeneration, with good perspectives for quick and reliable commercialization [8].
In literature, the expressions "rapid prototyping techniques" and "additive manufacturing" are often used as synonyms and generally refer to all those fabrication technologies where 3D structures are produced by adding material "layer-by-layer" [4],[32]. Each layer represents the cross-section of the 3D structure at a specific z-position [36]. These techniques offer the possibility of finely controlling the architecture of the scaffold (shape, size, pore interconnectivity, geometry and orientation). Biomimetic structures that vary in material composition and design can be obtained, thus improving the control of mechanical properties, biological response, and degradation rate of the scaffold [36].
Additive manufacturing technologies use different approaches, similar to each other in terms of the main procedures which are usually divided into 5 phases [37]:

1. Creation of the CAD model
2. Conversion of the CAD model into STL files
3. Slicing of the STL file
4. The additive manufacturing apparatus creates the scaffold layer-by-layer
5. Post-processing (e.g. sintering, if necessary)

The CAD file can be created by using a proper design software or obtained from magnetic resonance (MR) and computed tomography (CT) investigations, as both these imaging techniques allow obtaining accurate 3D reconstructions at high resolution [17]. If the CT images directly represent the patient's defect, one can create a 3D volumetric reconstruction of the bone defect to be treated in order to print a patient-specific scaffold (Figure 3) [36].

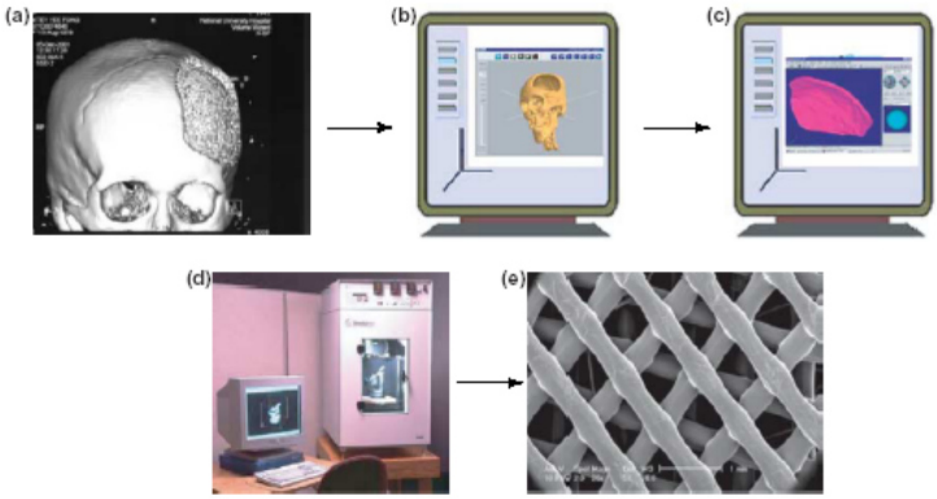

Figure 3. Steps required for scaffold manufacturing with additive manufacturing techniques that use CAD file. **a)** micro-CT imaging is used to generate a patient-specific CAD model of the bone defect. **b)** This is sent to the rapid prototyping system software to be "sliced" into thin layers. **c)** The "sliced" data are used as input instructions to the printing machine **d)** to build a scaffold **e)** according to a layer-by-layer deposition mode. Image adapted from Hutmacher et al. [36] with permission.

Another approach to scaffold fabrication is based on the use of hierarchal structures created by repeating a cell unit of known properties and geometry. However, this approach typically creates simple architectures with orthogonal and/or parallel channels, which do not really replicate the morphology of natural bone [38].

In order to overcome this limitation and, at the same time, create marketable shelves, CAD files from natural structures can be used to better imitate the trabecular structure of bone. Synthetic scaffolds inspired by natural structures are having a lot of success because they allow obtaining a much more biomimetic result. For example, the microstructure of cuttlefish bone has inspired the manufacture of bone tissue engineering shelves because its natural architecture is characterized by high porosity and at the same time high compressive strength [39].

In general, once the image is obtained, it is converted into DICOM (Digital Imaging and Communication Medicine) files and subjected to a segmentation process (a key step because the accuracy of the final model will depend on this) [17].

The reconstructed 3D volume is then used to create the 3D CAD model, which is converted into an STL file. The surface of the object is discretized using a polygonal mesh and cut into individual layers [40]. After checking and correcting possible errors in the STL file due to file conversion, all the individual parameters for 3D printing are selected and set. These will vary according to the type of technology adopted and the material chosen [17].

The setting of the layer thickness is a common parameter to all additive manufacturing systems as it will determine the resolution of the object [17].

Some variants of rapid prototyping technologies do not necessarily use the CAD file as an input, but the printing instructions and path may be all provided to the manufacturing apparatus by a text file (script). A relevant example is robocasting, by which a grid-like scaffold is built through the continuous extrusion of a thin filament (until 30 μm) containing ceramic (glass) particles from a nozzle onto a building platform [41].
Over the last two decades, more than 20 different additive manufacturing techniques have been used and marketed for tissue engineering applications [33],[36], and can be divided into three large families (Figure 4):

1) **Light/laser-based methods:** light or laser irradiation is used to fabricate cross-linked tissue engineering polymeric scaffolds or ceramic scaffolds in which the inorganic particles are bonded together by an organic binder that polymerizes during the process [33] .
   A typical set-up is usually composed of beam delivery optics, light source and the specific material [42]. The presence of a photoinitiator is required and must be added in small amounts to avoid toxicity [6]. Compared to other strategies, the main disadvantage of these methods is the lower cellular viability due to toxic residues, if not removed [43].

2) **Nozzle-based methods:** the material is extruded as a filament from a robot-controlled nozzle by applying a controlled pressure [6].
   These methods create continuous and thin streams of material that reproduce the CAD model and are directed by the software connected to the machine. Depending on the material chosen, these methods can also allow incorporating cells into the bioink. They must be subjected to low shear stress, which in turn has a positive effect on their capacity for diffusion and proliferation [6];

3) **Printer methods:** a head prints a liquid binder onto thin layers of powder, following the design that is generated by the software [33].
   Unlike nozzle-based methods, the biomaterial can be extruded as droplets and not as a continuous filament [6]. These methods use a non-contact technology based on the use of piezoelectric, thermal or electromagnetic forces to eject drops of material onto a building platform, thus replicating a CAD design [43]. Printer-based methods are relatively inexpensive and easily applicable to low-viscosity materials [6]. Based on several experiments, it can be stated that such procedures have good potential for bone tissue engineering applications [6]. However, due to frequent nozzle clogging, regular printing is difficult to achieve [6].

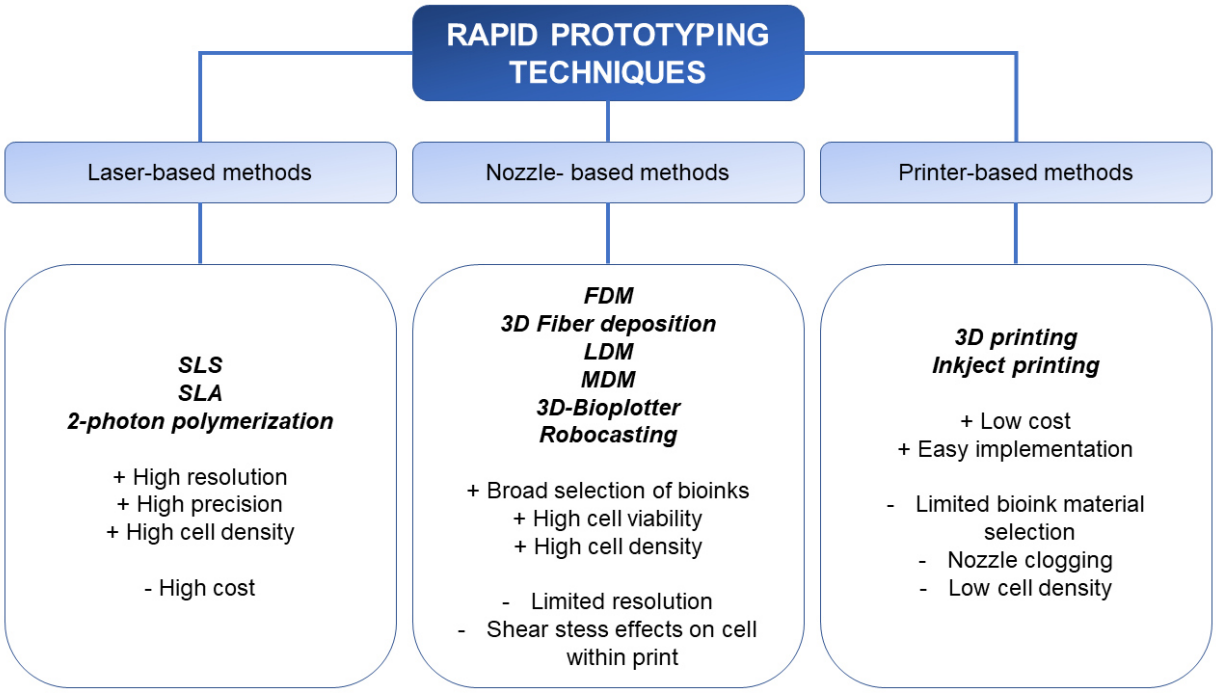

Figure 4. Rapid prototyping techniques and their advantages (+) and disadvantages (-). Select Laser Sintering, (SLS), Stereolithography (SLA), Fused Deposition Modelling (FDM), Low Temperature Deposition Manufacturing (LDM), Multi-nozzle deposition manufacturing (MDM).

Resolution is often the discriminating factor determining the choice of a specific technology rather than another one. Each method has a precise lower limit on the amount of detail which is capable of reproducing [33].

Table 4 provides a comprehensive picture of the additive manufacturing techniques that are commonly used for the production of tissue engineering scaffold.

Table 4. Comparison of different additive manufacturing technologies in bone tissue engineering (data from [1], [4], [34], [9]).

Technique	Process details	Resolution (μm)	Material for BTE	Advantages	Disadvantages
SLS	Preparing the powder bed Layer – by – Layer addition of powder Sintering each layer	500	Ceramics (HA β-TCP) Polymers (PLLA PCL) Metals	No need for support No – post processing	Dependency between Feature resolution and laser beam diameter Low surface quality Low mechanical strength

SLA	Immersion of a platform into aphotopolymer liquid Exposure to focused light according to the desired design Layer – by –layer fabrication	30	Ceramics (HA β-TCP, Bioactive glass) Polymers (PDLLA PPF)	Complex internal features Possible grow factors, proteins and cell patterning	Need for photopolymers High production cost Slow process
FDM	Strands of heated polymer/ceramics extrusion through a nozzle	250	Ceramics (HA TCP, Al_2O_3) Thermoplastic polymers	No need for platform/support Low production costs	Low surface quality Low resolution Low mechanicalproperties
3D printing	Strands of viscous material (in solution form) extrusion based on the predesigned structure Layer – by – layer deposition strands according to the tear of speed	100- 200	Ceramics (HA Bioactive glass) Polymers (PLA PEG PLGA)	Mild condition Possibility of plotting drugs and biomolecules No need for support material	Low mechanical strength Low accuracy compared to SLA Low surface quality (rough surface)
Robocasting	Direct writing of liquid using a small nozzle while a nozzle is moved across a platform.Consolidation through liquid – to gel transition Layer – by – layer fabrication.	100-1000	HA/PLA HA/PCL 6P53B glass/PCL	Independent 3D nozzle movement Precise control on thickness No need for platform /support	Material restriction Low accuracy compared to SLA
3D Fiber Deposition	The material is in a granule or pellet form. Material flow is regulated by applying pressure to the syringe	250	Polymers (PEGT)	Quick process	Need for high processing temperatures
LDM	The scaffold – building cycle is performed in a low – temperature environment under 0°C	300 - 500	Polymers (PLLA)	Possible incorporation of biomolecules	Use of solvents Need for freeze drying
MDM	It is similar to LDM But in this case a	400	Polymers (PLLA)	Enhanced range of materials	Need for solvents Need for freeze

	greater range of materials can be used			Incorporation of biomolecules	drying
3D Bioplotter	The nozzle system works pneumatically or via volume – driven injection. Key difference with other nozzle – based systems is the ability to plot into a liquid medium with matching density	45- 1600	Hydrogel Polymers (PCL PLLA)	Enhanced range of materials Incorporation of biomolecules	Low mechanical strength Low accuracy Slow processing

Several types of biomaterials can be processed by additive manufacturing technologies to fabricate bone-like scaffolds, including natural and synthetic polymers, ceramics and glasses [13], and even cells (bioinks) [9].
Among the techniques included in Table 4, the most suitable ones for the production of ceramic scaffolds are FDM, SLS, 3DP, robocasting and SLA, as summarized in Figure 5.

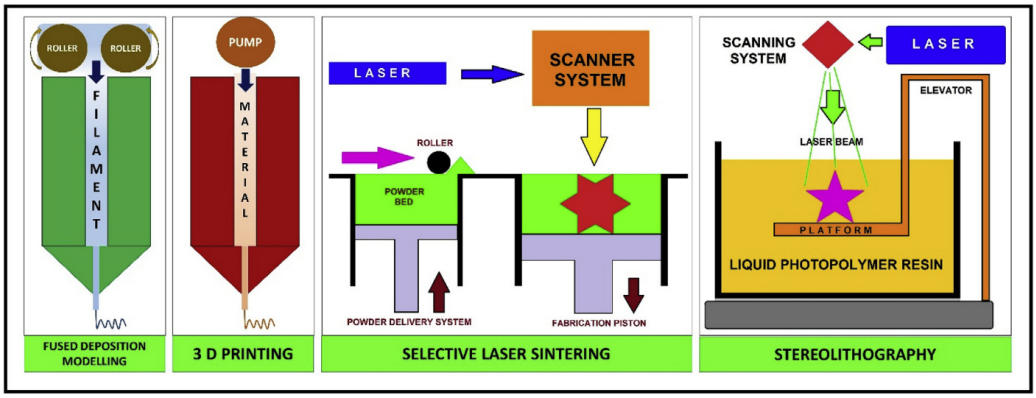

Figure 5. Schematic representation of the principal techniques used to produce ceramic scaffolds in bone tissue engineering. Image adapted from Mondal and Pal [7] with permission.

More specifically, it is possible to divide rapid prototyping techniques for the processing of bioceramic materials into two categories:

1) **Direct fabrication techniques:**
   These techniques allow the production of sintered ceramic components without the need for a subsequent thermal post-processing. According to this approach, the ceramic powders are melted using a high-energy laser [32]. However, rough surfaces are often obtained and local thermal stresses may arise. SLS technique or EBM (electron beam melting) are examples of direct techniques [32].

2) **Indirect fabrication techniques:**
These techniques are based on three fundamental steps: 3D printing, thermal de-binding, and sintering [32]. In these techniques, the printing process does not lead to a finished product but rather to the so-called "green body", which also contains a volatile organic binder in addition to the ceramic powder [40], [44]. Post-processing is therefore necessary to obtain the finished object with satisfactory mechanical properties and high relative density [44]. As a result, de-binding and sintering are crucial steps for defining the final properties of the scaffold. De-binding process leads to the thermal decomposition of the binder and then, by the sintering process, a final compact product, free of organic material is obtained [44]. Techniques such as FDM, SLA or 3D printing are part of this family [32].

The accurate internal architecture of the scaffold guaranteed by rapid prototyping techniques and the choice to use ceramic materials can indeed ensure producing structures of high interest for bone tissue engineering applications.
According to literature studies, among the available additive manufacturing technologies, SLA is one of the most promising due to the high resolution achievable and the possibility of using different kinds of ceramic materials [9]. Following the development of microstereolithography (MSTL) and Digital Light Process (DLP), the accuracy of the samples can be significantly improved and more complex structures can be successfully produced. Furthermore, SLA is suitable for the processing of methacrylate-based light curing composites commonly used in clinical practice without any modifications [32].

5. Stereolithographic methods

Among the various rapid prototyping techniques that can be used with ceramic materials, stereolithography (SLA) ensures maximum control in creating structures with a detailed and precise internal geometry and a high surface finish [1]. Developed in 1986 by Chuck Hull, who is considered the "father of 3D printing", SLA is one of the first techniques to appear on the market [1]. Since then, SLA has been widely used in bone tissue engineering for the production of hydroxyapatite, β-TCP, zirconia, alumina, and bioactive glass scaffolds [1].

5.1 Processing

SLA is an additive manufacturing process using a bath of UV-curable photosensitive liquid, an ultraviolet (UV) laser to build 3D structures layer-by-layer, a movable platform and a dynamic mirror system [1], [33]. When the printing process begins, the laser beam solidifies the photosensitive liquid at the surface of the bath, thus creating the first layer; the irradiated zones are defined in accordance with the previously determined CAD model of the scaffold [45],[36]. If ceramic particles are dispersed in the liquid, it acts as a binder and, once polymerized, glues the particles together. When the irradiation

of a layer ends, depending on the configuration of the machine (top-down or bottom-up system, see Figure 6), the slurry bed is respectively raised or lowered by an elevator platform.
Most SLA apparatuses use the bottom-up system; in this case the platform moves down so that the new material can cover the newly formed layer, and the laser cures a new layer over the previous one [1]. In the second system the platform moves upwards and the vat must be completely transparent [9]. The latter has a few more advantages compared to the bottom-up system, first of all the demand for a smaller amount of raw material [9].

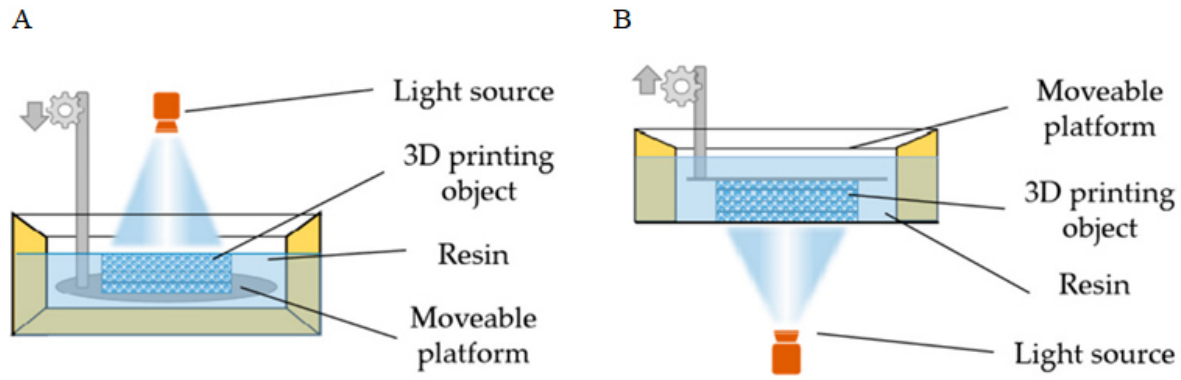

Figure 6. Stereolithography with A) bottom-up system; B) top-down system. Image reproduced from Mao et al. [46] under the Creative Common Attribution Licence (CC BY 4.0).

The displacement along the z-axis and the irradiation depth determine the thickness of each single layer, and thus the surface resolution of the final object [1]. Exposure to the UV laser light solidifies the pattern traced on the slurry and allows it to adhere to the layer below [33]. The subsequent deposition of adjacent layers leads to the building of the 3D object characterized by highly-resolved solid structure [47].

5.2 The slurry: composition and characteristics

Long-term stability and suitable rheological behaviour are two of the most relevant characteristics that a ceramic slurry should exhibit to achieve a smooth printing flow [1]. Most of the slurries used are non-aqueous suspensions, because water-based suspensions usually give rise to weak structures; it is therefore preferable to use acrylamide resin-based slurries [1].
From a rheological point of view, slurries should exhibit Newtonian flow behaviour [48] and viscosity values should be low enough to facilitate the printing process and to avoid the formation of air bubbles [49]. Slurry viscosity is strictly dependent on the concentration of ceramic particles. In order to obtain high-quality products, the percentage of ceramic powder in green bodies should be at least 50% [49]; as the particle content increases, shrinkage decreases upon sintering, thus significantly improving the quality of the final product [40].

However, if the powder content is too high, viscosity could increase over the optimal value established for the processing of ceramic materials (3 Pa·s) [49]. Moreover, particles should be homogeneously dispersed within the organic liquid and their size should be smaller than the layer height [1].
It is possible to reduce the slurry viscosity by incorporating non-reactive "thinners" (e.g. N-methylpyrolidone) or by increasing the manufacturing temperature [40]. Moreover, the addition of some dispersant agents could be beneficial to the slurry quality, ensuring low viscosity values and good homogeneity while keeping the solid loading high [50]. Specifically, long-chained fatty acids, phosphine oxides or oligomeric surfactants can reduce particle agglomeration, thereby decreasing viscosity and improving slurry stability and density [40].
Transparency to UV light is another key requirement in order to achieve the desired light penetration depth. In fact, if the slurry is not transparent enough, light penetration will be attenuated, resulting in a considerable cure depth decrease. If required, absorbant agents for visible or UV light could be added in order to limit the cure depth, thus avoiding an excessive polymerisation along the z-axis [40].

5.3 The photopolymerization process: chemical basis

When the ceramic powder, monomer, and photoinitiator are exposed to the UV light, the photoinitiator generates cation species or free radicals attacking the double bonds of the monomer and triggering polymerisation [49]. The subsequent reactions between the monomer and the active end of the chain allow the polymeric chains to increase their length until a termination reaction occurs [49].
Two different types of photopolymerisation can occur: cationic polymerisation or radical polymerization. The latter is generally preferred in SLA processes because it is easier to control [49].
During radical polymerization, the photoinitiator divides and generates radical species. These radicals are extremely reactive and immediately attack the double bonds of the monomer [49]. The main steps of radical polymerisation are given below [49]:

Initiation $$PI \xrightarrow{h\nu} R\cdot \quad (1)$$

Propagation $$R\cdot + M \rightarrow R(M)_{n}\cdot \quad (2)$$

Termination $$R(M)_{n}\cdot + R(M)_{m}\cdot \rightarrow R(M)_{n+m}\cdot R \qquad R(M)_{n}\cdot \rightarrow R(M)_{n} \quad (3)$$

hv

M= monomer, R= radical, PI= photoinitiator

For radical photopolymerisation, acrylate functionalised monomers (e.g. cured acrylated epoxy, acrylated polyester and acrylated urethane) and telechelic oligomers are usually used due to the rapid

rate of their polymerisation [49]. Acrylates are often combined with methacrylates to decrease shrinkage during curing. Another method to reduce shrinkage and speed up curing may be a combination of acrylate and epoxy-based resins [40]. The photopolymer acts as binder between the ceramic powder, making it possible to accurately manufacture the part [44].
The kinetic of reaction and the mechanical properties of the final structure are significantly affected by the quantity of photoinitiator and its selection has to be based on the nature of the monomers used. It has been reported that, as the photoinitiator concentration increases, the polymerisation speed and the stiffness of the sample increase as well [40].
However, the quantity of photoinitiator must be limited as their intrinsic cytotoxicity could be harmful for tissue ingrowth and regeneration; for example, photoinitiators for cationic polymerisation form strongly acidic protons (H^+) and it is therefore preferable not to use them for biomedical applications. For this reason, radical photoinitiators are usually preferred, although serious DNA damages could occur if not properly dosed [40]. A commonly-used low-toxicity photoinitiator is Irgacure 2959 [40].

5.4 Key parameters for the photopolymerization process

Some important parameters need to be set and controlled in order to obtain a good light-curing slurry for printing, as described in the following sections.

5.4.1 Energy of the UV Laser

The energy of the UV source can be calculated as the product between the intensity of the UV light beam and the exposure time [51]. The incident energy dose must be adjusted in order to achieve the correct depth of cure, coinciding with the desired layer thickness [51].
For a single mode laser beam, the intensity follows a Gaussian distribution [51]. A Gaussian beam of peak intensity I_{max} and width w^2_{Gauss} has an actual distribution of intensity at the surface (z = 0) which varies along the y axis, according to equation *(4)*:

$$I_0(y, z = 0) = I_{max} exp\left(\frac{-2y^2}{w^2 Gauss}\right) \quad (4)$$

where z represents the depth from the surface of the suspension and y is the distance from the centre of the beam.

The incident energy dose (E_0) can be calculated as t·I (t illumination time, I intensity) *(5)*:

$$E_0(y, z=0) = t \cdot I_{max} exp\left(\frac{-2y^2}{w^2_{Gauss}}\right) \quad (5)$$

At any point, the incident energy dose ($E(z)$) can be estimated by Beer-Lambert's law, which states that the energy dose is attenuated logarithmically as a function of depth (z), according to equation *(6)* [51]:

$$E(z) = E_0 exp\left(\frac{-z}{S_d}\right) \quad (6)$$

where E_0 is the dose of incident energy on the surface and S_d is the resin sensitivity in the depth direction.

The energy dose could be estimated by equation *(7)*:

$$E(z) = E_{max}\, exp\left(\frac{-2y^2}{w_{Gauss}^2}\right) exp\left(\frac{-z}{S_d}\right) \quad (7)$$

where E_{max} is the maximum dose of energy.

The polymerisation of the slurry will take place at every point in which the energy dose is greater than or equal to the critical energy dose necessary for polymerisation to take place (E_d) [51]: polymerisation in the cross-section must then take place at points (y*, z*), where $E(y^*, z^*) = E_d$.

We will thus obtain a parabolic curve shape given by equation *(8)* [51]:

$$ln\left(\frac{E_{max}}{E_d}\right) = \frac{2y^{*2}}{w_{Gauss}^2} + \frac{z*}{S_d} \quad (8)$$

5.4.2 Penetration depth (D_p)

The penetration depth of the laser beam (D_p) is defined as the depth where intensity is reduced by 1/e of the beam intensity measured at the bath surface [45], [47]. D_p depends on the size and quantity of the ceramic particles [49] and the difference in refractive index between the UV curable solution and the ceramic powder [52]. Once E_d and D_p are determined, it is possible to properly choose the laser beam power and the scanning speed [53].

A good slurry for SLA is usually characterized by high D_p values, in order to minimise the layer thickness, and low E_d so that the polymerization reaction can be initiated with a low energy dose [54].

5.4.3. Cure width (C_w) and cure depth (C_d)

The curing width (C_w) is always greater than the diameter of the laser beam due to dispersion phenomena caused by the presence of ceramic particles [55].

Cure depth (C_d) is defined as the maximum depth at which the material receives sufficient light to reach the gel point [49], forming a three-dimensional gel network during light-curing [47]. The gel point indicates the transition of the slurry from visco-plastic (pre-gel) to rigid-elastic (post-gel) behaviour [56]. C_d must be at least equal to the layer thickness [56] and, if the polymerization depth is too large, loss in spatial resolution could be observed.

C_d can be related to the parameters of Beer-Lambert's law according to equation *(9)*:

$$C_d = S_d\, ln\left(\frac{E_0}{E_d}\right) \quad (9)$$

It is essential to understand how the composition of the slurry influences the relationship between C_d and energy dose in order to obtain photopolymerizable slurries [56]. A compromise between these two parameters must be established so that products with both satisfactory spatial resolution and low manufacturing times can be obtained [51]. High C_d values require high energy density but guarantee an optimization of the working time; on the contrary, a good resolution would require low energy density [55].
It has been confirmed that, by varying the concentration of the ceramic powder, the particle size, and the refractive index, both C_d and C_w could be properly modified, according to the needs [51].
The curing rate increases as the ratio of the refractive index between ceramic particles and polymeric binder decreases. The ceramic powder scatters light, thus decreasing the resolution and cure depth, and increasing printing time [1]. Smaller particles generally have better light scattering properties [1].
Gentry and Halloron have shown that when the refractive index of the precursor monomer corresponds to the refractive index of the ceramic powder, there is an improvement in curing depth [49].
Light scattering effects lead to the polymerisation of an area larger than the predetermined area: this effect is called overgrowth [57].
C_d also depends on how much photoinitiator is used for slurry preparation: if the photoinitiator concentration is high, C_d decreases [47].

5.5 Post-processing

Unlike SLS and other direct techniques, where the ceramic material is shaped and sintered in a single step, SLA requires a further step called post-processing once printing is concluded. In fact, the so-called "green body" resulting from the printing process still has to be consolidated by thermal treatments to be transformed into a ceramic part [44], [57].
Besides the ceramic powder (typically ~60%), the "green body" still contains a volatile organic matrix which must be eliminated [40], [44]. The post-processing stage involves three fundamental steps: cleaning and drying of pieces from uncured slurry, de-binding and sintering. During de-binding, the binder is thermally decomposed: organic residuals slowly degrade, leaving behind only the loosely compacted ceramic powder [44]. During de-binding, the temperature increase must be slow and constant to avoid the formation of internal stresses which can result in the formation of cracks within the structure [44]. The de-binding temperature and time required depend on several factors, such as quantity of organic components, composition of organic components, size and distribution of ceramic particles, and percentage of solid part contained in the slurry as compared to the organic matrix [58]. Binder removal is a key stage in order to avoid contaminations that could change the properties of the final product [9].
The greens are then densified by sintering to form the final ceramic scaffold [44]. The high-temperature sintering process is usually carried out between 50-75% of the melting temperature of the material [9]. Usually, the higher the sintering temperature, the more resistant the final scaffold [7]. However, if the porosity of the sintered scaffold remains too high, the mechanical properties may be affected significantly anyway [9]. During sintering, the scaffold inevitably undergoes volumetric shrinkage [9] that must be carefully considered and preferably estimated before printing at the design stage [32].
The main steps of the post-processing are shown in Figure 7.

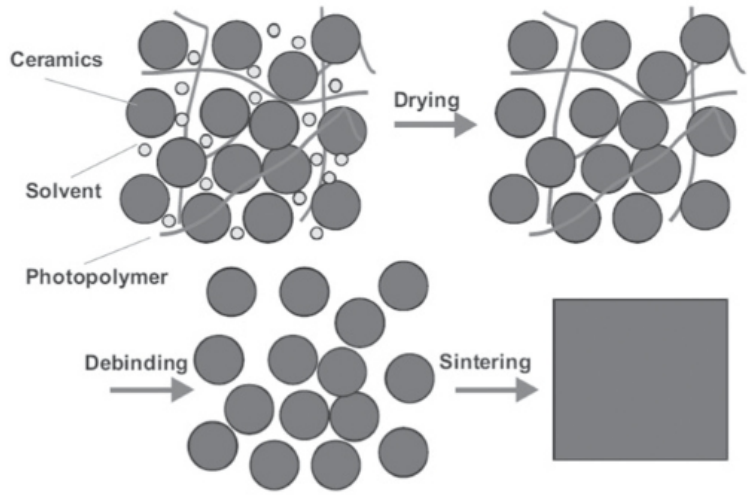

Figure 7. Main steps of post-processing from the ceramic green body to the sintered dense ceramic. Image reproduced from Lantada et al. [44] under the Creative Commons Attribution Licence (CC BY 3.0).

In order to minimize shrinkage and increase shape accuracy, the slurry should have a high ceramic particle content (solid loading); however, this can cause the formation of cracks due to gases which are unable to reach the surface of the scaffold, creating a strong internal pressure [1]. The sintering process can be facilitated by applying an external pressure (sintering under pressure). On the contrary, if no external pressure is applied, the sintering is called "sintering without pressure" (or conventional or pressureless sintering) [9].

5.6 SLA: Advantages and disadvantages

Some more advanced variants, such as microstereolithography (μ-SLA) and two-photon polymerization (TPP), allow an even better quality resolution compared to conventional SLA [9].
With μ-SLA, the thickness of a layer can be decreased up to 10 μm [9], whereas TPP is even capable of achieving a resolution of less than 0.1 μm [40]. Resolution of a standard SLA layer depends on the elevator layer resolution (up to 1.3 mm) and laser spot size (80-250 mm) [36].
Products made by SLA are usually robust and can be used as master patterns for thermoforming, selection moulding, as well as in various metal casting processes [33]. However, this process often has high processing costs: the photo-curable resin can cost from $300 to $800 and a SLA apparatus can cost from $100.000 to more than $500.000 [33].
If the product is very large, point-by-point polymerization of the cross-section of each layer can be very time-consuming, thus making the process computationally long and demanding [40].
In summary, the main parameters that influence the success of SLA printing include type and concentration of monomer, volume ratio between ceramic powder and organic components, chemical

interaction between ceramic powder and organic components, viscosity of the slurry, laser beam power, optimisation of de-binding and sintering steps, and time of exposure to light [1].

6. The latest frontier: digital light processing (DLP)-based stereolithography

Recently, a new method based on the SLA technique has been proposed, which allows a considerable reduction in production time. Digital light processing (DLP)-based SLA is an innovative and very efficient rapid prototyping technology particularly appreciated for the production of calcium phosphate scaffold for bone tissue engineering. Besides its high speed, DLP guarantees an excellent resolution of the final product [59] and reduces the stress to which samples are subjected during processing [60].
The term DLP refers to digital mirror devices that, when properly controlled, selectively expose the photosensitive resin to visible or UV light [61]. The manufacturing process is similar to the classical SLA: the DLP builds complex 3D layer-by-layer structures and the geometry of the various layers is previously determined by cutting the design CAD model on a series of horizontal planes at close range [45]; the operator is also able to set all printing parameters according to the slurry curing characteristics [57]. The major difference compared to classical SLA is the use of a series of computer-programmable arrays of digital micro-mirror devices (DMD) [45], which allow the simultaneous irradiation of the entire desired cross-section [40], [59].

6.1 System setup

The main components of the DLP system include the digital micro-mirror devices (DMD), a projection lens, a vat containing UV curable resin, a UV light source, and a motorised translation stage. The setup can be implemented in two different ways: a free-surface approach or top-down projection (Figure 8.A)) and a constrained surface approach or bottom-up projection (Figure 8.B)) [40],[62].
In a free-surface approach, the light exposure is from above and the building platform is immersed in a slurry bath. After the polymerisation of a layer, the z-stage is lowered into the resin tank and the new material successively coats the growing part [45].
If a constrained surface approach is adopted, the slurry is illuminated from below through a transparent vat. After the polymerisation of each layer, the building platform is raised by a distance equal to the thickness of the individual layer. In this way, the liquid slurry can flow into the cavity and the next layer is created [62].

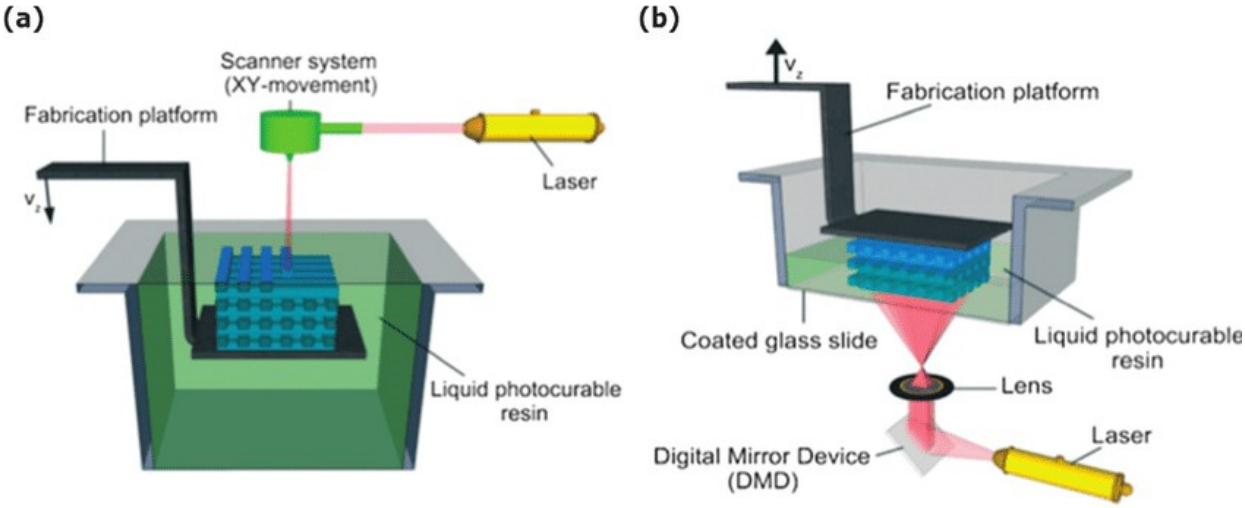

Figure 8. DLP setup for (a) free surface approach (top down) and (b) constrained surface approach (bottom up). Figure adapted from Ko et al. [62] under the terms of the Creative Commons CC BY license.

A constrained surface approach is often preferred as it guarantees certain advantages over the other method, including increased motion accuracy of the z-stage down to precisions of 0.1-1 µm which ensures a smooth surface and precise layer thickness [40], and the possibility of adding new liquid slurry if needed through a pump (fresh material supply is always guaranteed, even for large jobs) [62]. Furthermore, the layer created is not directly exposed to air, allowing faster light-curing [62], and the structure under construction is not completely submerged in the vat, which considerably reduces the amount of material required and, consequently, the cost of production [40].
It is important for the newly created layer not to remain attached to the surface of the vat, but to properly adhere to the previous layer, and for the whole structure to remain firmly attached to the building platform throughout the process. In order to promote the attraction forces between scaffold and building platform and reduce the attraction forces between scaffold and vat surface, the vat is coated with hydrophobic films, such as polytetrafluoroethylene (PTFE) or polydimethylsiloxane (PDMS) [62].
Furthermore, it is necessary to pay attention to any curved surfaces during printing: the DLP process is particularly suitable for illuminating geometries with 90° angles and may carry the risk of creating saw-tooth roughness when illuminating curved structures [40].

6.2 Digital micro-mirror device (DMD)

Digital micro-mirror device (DMD) is the key component of the DLP process. A microelectromechanical system (MEMS) acts as a dynamic mask when connected to the computer [40]. The chip was developed at Texas Instruments in 1987 and consists of an array of reflective aluminium micro-mirrors [45]. Each mirror is fixed on top of a yoke and hinge system on a silicon memory cell, creating a single pixel [40]. If a sufficiently high polarization voltage is applied, the electrostatic attractions bring the mirrors into an unbalanced position of <10° or >10° with respect to the position of

equilibrium [63]. The address voltage determines in which direction the mirror is tilted [40]. If the micro-mirror is in the condition of <10° ("tilt on"), the light from the light source is reflected in the projection lens and the image is created [63]. When it is in the condition of >10° ("tilt off"), the light is not reflected but is collected by a light absorber [63]. Generally, a DMD chip contains more than 442.000 switchable mirrors [63].
The use of the DMD provides many advantages: first, the large number of micro-mirrors allow a better and more uniform intensity of the light [45] and the pixels, being reduced in size, allow a higher resolution of the display [45]. Furthermore, ultra-flat aluminium micro-mirrors permit successful modulation of the UV illumination [45]. There is also a greater control over exposure time: this is particularly important so that the modulation of the grayscale intensity can occur at pixel level [45].
In summary, the DLP process exhibit interesting advantages as compared to other rapid prototyping techniques, including high spatial resolution due to the small size/large number of pixels [50], no need for special environmental conditions during processing [61], and high processing speed. As regards the last point, the use of dynamic masks, which allow the polymerisation of an entire cross-section at once, drastically reduces the fabrication time regardless of the shape, size and complexity of the structure to be reproduced [61]. The high speed of the process not only carries an economic advantage but is a fundamental requirement when working with partially stable resins that necessarily require fast processing times [40]. By using the constrained surface approach, the amount of material required is much smaller compared to free surface approach and this further contributes to lower production costs [61].
Nonetheless, there are also some critical aspects about this technique, including undesirable diffusion of light through the previously formed layers, which might cause uncontrolled polymerization and occlusion of the pore [64], and the need for properly controlling the curing depth of the UV light in order to avoid loss of resolution [64].

7. Current applications of SLA- and DLP-derived ceramic scaffolds

In recent years conventional SLA and DLP process have established themselves as successful techniques for the manufacturing of ceramic scaffolds, owing to the possibility of producing dense, precise and high-strength ceramics [65]. These techniques allow greater flexibility in the realization and modification of designs; samples can be quickly tested and readjusted and parts with precise characteristics can be created [65]. These attractive properties have allowed obtaining good results not only in bone tissue engineering but also in dentistry and cranio-maxillofacial procedures [65]. Additive printing based on SLA and high-resolution DLP allow fabricating ceramic products with theoretical densities higher than 99.8%, good mechanical properties, and homogeneous, precise and highly reproducible microstructure [65].
A wide range of ceramic materials can be processed, such as zirconia (ZrO_2), alumina (Al_2O_3), calcium phosphates and hydroxyapatite [65]. Ronca et al. developed a composite shelf applying SLA to nano-hydroxyapatite and poly-(DL-lactide). Due to the presence of hydroxyapatite, the scaffold had a higher structural strength and better biocompatibility with bone cells [37].

Brie et al. created pure hydroxyapatite scaffolds by SLA and implanted them in the skull of 8 human patients. After a 12-month follow-up, these scaffolds did not cause any complications and a perfect continuity between host tissue and implant was observed [37].

Mangano et al. showed that biphasic calcium phosphate scaffolds made by SLA had better characteristics than scaffolds obtained via foaming and traditional sintering. Porous cylindrical scaffolds were composed of 30% of hydroxyapatite and 70% β-TCP in order to find the right balance for bone regeneration favoured by the rapid resorption of β-TCP and low resorption of hydroxyapatite [66]. The scaffolds obtained by SLA were more effective in mimicking the porous trabecular organization of the maxillary bone characterized by high interconnectivity of void spaces. SLA-moulded specimens had a higher final strength with a smaller plastic region. An average compressive of about 6.4 MPa and a total compressive deformation of about 3.6% were recorded prior to achieving material fracture [66].

Hydroxyapatite cylindrical scaffolds were fabricated through DLP by Tesavibul et al. The samples had a geometry comparable to that of the original CAD model (11.3 mm diameter and 3 mm thickness). The density of the solid skeleton reached 91% of the theoretical one and the scaffold compressive strength was 0.36 MPa; the average pore size was between 500-700 μm. Good results were obtained from in vitro biocompatibility tests: after 14 days, preosteoblastic MC3T3-E1 cells seeded on the scaffolds began to proliferate and differentiate into an osteoblastic lineage [67].

Several studies for the production of scaffolds using bioresorbable ceramics were recently made by Lithoz GmbH (Austria) using their own CeraFab DLP process system. In 2019, β-TCP-based bone tissue engineering shelves were printed in different geometries (hexagonal Kagome, rectilinear Grid, Schwarz primitive, and hollow Schwarz architecture) to evaluate the best compromise between porosity and mechanical properties [59]. The rectilinear Grid structure showed a compressive strength of 44.7 MPa (Weibull modulus 5.28) with 50 vol.% porosity [59].

Despite the good results that are being obtained towards “ideal” tissue engineering scaffolds, pore microstructure defects, rheological properties of the slurry, correct sintering temperature and satisfactory mechanical properties are still partially open issues that need to be improved [68]. In any case, the various studies have shown that it is almost always possible to obtain scaffolds with high relative density and excellent cell biocompatibility. The main property that should be improved is the compressive strength of the sample, often too low for the requirements of bone scaffolds. For example, 45S5 Bioglass® scaffolds obtained by DLP process have a lower compressive strength than porous glass foams produced by sponge replication [69].

Table 5 collects a selection of studies found in the literature and the main characteristics of scaffolds printed with classical SLA or DLP technique.

Table 5. Overview of bioceramic scaffolds fabricated by SLA/DLP process

Reference	Material	Scaffold geometry	Technique	Scaffold properties
Mangano et al., 2019 [66]	Biphasic calcium phosphate (70% β-TCP/ 30% hydroxyapatite)	Porous cylinders	SLA	- Pore size: 100 µm - Compressive strength: 6.4 MPa - Biocompatible (cell-culturing with MC3T3-E1 pre-osteoblasts)
Tesavibul et al., 2014 [67]	Hydroxyapatite	Porous cylinder	DLP	- Relative density: 91% - Pore size: 500-700 µm - Biocompatible (cell-culturing with MC3T3-E1 pre-osteoblasts)
Schimidleithner et al., 2019 [59]	TCP	Grid structure	DLP	- Relative density: 99.5% - Pore size: 400 µm - Porosity: 50 vol.% - Compressive strength:44.7 MPa and Weibull modulus: 5.28 - Biocompatible (cell-culturing with MC3T3-E1 pre-osteoblasts)
Yao et al., 2019 [68]	Hydroxyapatite	Cubic structure (10 x10 x 10 mm^3)	DLP	- Relative density: 95.85% - Shear viscosity < 3.7 Pa·s
Ghayor et al., 2018 [70]	TCP	15 scaffolds with different defined pore/bottleneck dimensions and distributions	DLP	- Pore size: 700-1200 µm
Zeng et al., 2018 [60]	Hydroxyapatite	Square pore structure (21 x 21 x 3 mm^3)	DLP	- Compressive strength (z-direction): 11.8 MPa - Compressive strength (x-direction): 5.1 MPa - Biocompatible (cell-culturing with MC3T3-E1 pre-osteoblasts)
Tesavibul et al., 2012 [69]	45S5 Bioglass®	Cylindrical cellular structure (d=9.8 mm; h=11.6 mm)	DLP	- Pore size: 500 µm - Compressive strength of the cellular structure: 0.33 MPa
Liu et al., 2019 [71]	Hydroxyapatite	Porous rectangular scaffold (L= 10 mm; h=20 mm)	DLP	- Pore size: 300-600 µm - Relative density: 94.9% - Porosity: 49.8 vol.% - Bending strength: 41.3 MPa - Compressive strength: 15.25 MPa - Biocompatible (cell-culturing with MC3T3-E1 pre-osteoblasts)
Feng et al., [72]	Hydroxyapatite (45 vol.%)	Porous cylindrical scaffold (d=11.8; h=14.2)	DLP	- Relative density: 66.6% - Flexural strength: 10.0 MPa - Compression strength: 12.0 MPa

Cao et al., 2020 [73]	ZrO_2 / hydroxyapatite	Porous rectangular scaffold (L=7.5 mm; h=15 mm)	DLP	- Compressive strength (hydroxyapatite 10 wt.%): 52.25 MPa - Biocompatible (cell-culturing with MC3T3-E1 pre-osteoblasts)

8. Conclusions

In order to overcome the intrinsic drawbacks of natural grafts (transplant materials), during the last decades bone tissue engineering focused on the development of man-made ceramic scaffolds. These synthetic grafts aim at providing the same function as ECM, thus ensuring cellular activity, adequate mechanical support and proper mechanical and biochemical interactions with cells and proteins. In order to perform these tasks, the scaffold must be carefully designed: in fact, it is not sufficient to choose a biocompatible material, but a minimum degree of porosity (50-60 vol.%), pore interconnectivity and adequate surface characteristics should be achieved to promote effective osteogenesis.

Over the years, many techniques have been developed and improved for this purpose, and additive manufacturing technologies allow obtaining scaffolds with a highly reproducible and customizable structure. These methods rely on the reproduction of CAD files and are able to build 3D porous scaffolds with well-controlled structural properties. Among the various additive manufacturing techniques, SLA is very suitable to be used with ceramic materials, ensuring a very high resolution and ease of processing. At present, this technique has been further improved by replacing UV laser with a new lighting method, called DLP, that is based on a DMD consisting of millions of mirrors and is able to reduce processing time without affecting the spatial resolution. Processing bioceramics with SLA strategies is a winning combination leading to produce high-quality and accurate scaffolds that can be used to manage both small and large bone defects even in load-bearing anatomical sites.

References

[1] K. Lin, R. Sheikh, S. Romanazzo, and I. Roohani, "3D printing of bioceramic scaffolds-barriers to the clinical translation: From promise to reality, and future perspectives," Materials (Basel)., vol. 12, no. 7, pp. 1–20, 2019.

[2] L. C. Gerhardt and A. R. Boccaccini, "Bioactive glass and glass-ceramic scaffolds for bone tissue engineering," Materials (Basel)., vol. 3, no. 7, pp. 3867–3910, 2010.

[3] S. Dorozhkin, "Medical Application of Calcium Orthophosphate Bioceramics," Bio, vol. 1, no. 1, pp. 1–51, 2011.

[4] W.-Y. Yeong et al., "Rapid prototyping in tissue engineering: challenges and potential," Trends Biotechnol., vol. 22, no. 12, pp. 643–652, 2004.

[5] K. Rezwan, Q. Z. Chen, J. J. Blaker, and A. R. Boccaccini, "Biodegradable and bioactive porous polymer/inorganic composite scaffolds for bone tissue engineering," Biomaterials, vol. 27, no. 18, pp. 3413–3431, 2006.

[6] L. Zhang, G. Yang, B. N. Johnson, and X. Jia, "Three-dimensional (3D) printed scaffold and material selection for bone repair," Acta Biomater., vol. 84, pp. 16–33, 2019.

[7] S. Mondal and U. Pal, "3D hydroxyapatite scaffold for bone regeneration and local drug delivery applications," J. Drug Deliv. Sci. Technol., vol. 53, pp. 1–11, 2019.

[8] H. E. Jazayeri et al., "The cross-disciplinary emergence of 3D printed bioceramic scaffolds in orthopedic bioengineering," Ceram. Int., vol. 44, no. 1, pp. 1–9, 2018.

[9] F. Baino et al., "Processing methods for making porous bioactive glass-based scaffolds—A state-of-the-art review," Int. J. Appl. Ceram. Technol., vol. 16, no. 5, pp. 1762–1796, 2019.

[10] ASTM International Standard Guide for Characterization of Ceramic and Mineral Based Scaffolds used for Tissue-Engineered Medical Products (TEMPs) and as Device for Surgical Implant Applications and ASTM Standard F2883 - 11, "Standard Guide for Characterization of Ceramic and Mineral Based Scaffolds used for Tissue-Engineered Medical Products (TEMPs) and as Device for Surgical Implant Applications," ASTM B. Stand., no. January 2012, pp. 1–7, 2011.

[11] C. M. Murphy, F. J. O'Brien, D. G. Little, and A. Schindeler, "Cell-scaffold interactions in the bone tissue engineering triad," Eur. Cells Mater., vol. 26, pp. 120–132, 2013.

[12] A. R. Amini, C. T. Laurencin, and S. P. Nukavarapu, "Bone tissue engineering: Recent advances and challenges," Crit. Rev. Biomed. Eng., vol. 40, no. 5, pp. 363–408, 2012.

[13] Y. J. Seol, D. Y. Park, J. Y. Park, S. W. Kim, S. J. Park, and D. W. Cho, "A new method of fabricating robust freeform 3D ceramic scaffolds for bone tissue regeneration," Biotechnol. Bioeng., vol. 110, no. 5, pp. 1444–1455, 2013.

[14] G. Turnbull et al., "3D bioactive composite scaffolds for bone tissue engineering," Bioact. Mater., vol. 3, no. 3, pp. 278–314, 2018.

[15] E. Babaie and S. B. Bhaduri, "Fabrication Aspects of Porous Biomaterials in Orthopedic Applications: A Review," ACS Biomater. Sci. Eng., vol. 4, no. 1, pp. 1–39, 2018.

[16] K. Doi et al., "Development of Implant/Interconnected Porous Hydroxyapatite Complex as New Concept Graft Material," PLoS One, vol. 7, no. 11, pp. 1–10, 2012.

[17] D. Martinez-Marquez, A. Mirnajafizadeh, C. P. Carty, and R. A. Stewart, Application of quality by design for 3D printed bone prostheses and scaffolds, vol. 13, no. 4. 2018.

[18] I. Denry and L. T. Kuhn, “Design and characterization of calcium phosphate ceramic scaffolds for bone tissue engineering,” Dent. Mater., vol. 32, no. 1, pp. 43–53, 2016.
[19] J. Henkel et al., “Bone Regeneration Based on Tissue Engineering Conceptions-A 21st Century Perspective,” Bone Res., vol. 1, pp. 216–248, 2013.
[20] X. Du, S. Fu, and Y. Zhu, “3D printing of ceramic-based scaffolds for bone tissue engineering: An overview,” J. Mater. Chem. B, vol. 6, no. 27, pp. 4397–4412, 2018.
[21] Q. Z. Chen and G. A. Thouas, “Fabrication and characterization of sol-gel derived 45S5 Bioglass®-ceramic scaffolds,” Acta Biomater., vol. 7, no. 10, pp. 3616–3626, 2011.
[22] A.R. Boccaccini, M. Erol, W.J. Stark, D. Mohn, Z. Hong, J.F. Mano, Polymer/bioactive glass nanocomposites for biomedical applications: a review, Composites science and technology, 70 (2010) 1764-1776.
[23] K. Szustakiewicz et al., “The influence of hydroxyapatite content on properties of poly(L-lactide)/hydroxyapatite porous scaffolds obtained using thermal induced phase separation technique,” Eur. Polym. J., vol. 113, no. January, pp. 313–320, 2019.
[24] V. Maquet, A. R. Boccaccini, L. Pravata, I. Notingher, and R. Jérôme, “Porous poly(α-hydroxyacid)-bioglass composite scaffolds for bone tissue engineering,” Biomaterials, vol. 25, no. 18, pp. 4185–4194, 2004.
[25] M. Degli Esposti, F. Chiellini, F. Bondioli, D. Morselli, and P. Fabbri, “Highly porous PHB-based bioactive scaffolds for bone tissue engineering by in situ synthesis of hydroxyapatite,” Mater. Sci. Eng. C, vol. 100, no. February, pp. 286–296, 2019.
[26] O. Bretcanu et al., “Electrospun nanofibrous biodegradable polyester coatings on Bioglass®-based glass-ceramics for tissue engineering,” Mater. Chem. Phys., vol. 118, no. 2–3, pp. 420–426, 2009.
[27] Y. Hong et al., “Preparation, bioactivity, and drug release of hierarchical nanoporous bioactive glass ultrathin fibers,” Adv. Mater., vol. 22, no. 6, pp. 754–758, 2010.
[28] F. Baino, G. Novajra, and C. Vitale-Brovarone, “Bioceramics and scaffolds: A winning combination for tissue engineering,” Front. Bioeng. Biotechnol., vol. 3, no. December, pp. 1–17, 2015.
[29] Q. Fu, M. N. Rahaman, B. Sonny Bal, R. F. Brown, and D. E. Day, “Mechanical and in vitro performance of 13-93 bioactive glass scaffolds prepared by a polymer foam replication technique,” Acta Biomater., vol. 4, no. 6, pp. 1854–1864, 2008.
[30] Q. Z. Chen, I. D. Thompson, and A. R. Boccaccini, “45S5 Bioglass®-derived glass-ceramic scaffolds for bone tissue engineering,” Biomaterials, vol. 27, no. 11, pp. 2414–2425, 2006.
[31] G. Tripathi and B. Basu, “A porous hydroxyapatite scaffold for bone tissue engineering: Physico-mechanical and biological evaluations,” Ceram. Int., vol. 38, no. 1, pp. 341–349, 2012.
[32] R. Gmeiner et al., “Additive manufacturing of bioactive glasses and silicate bioceramics,” J. Ceram. Sci. Technol., vol. 6, no. 2, pp. 75–86, 2015.
[33] E. Mancuso, N. Alharbi, O. Bretcanu, M. Marshall, M.A. Birch, A.W. McCaskie, et al. Three dimensional printing of porous load-bearing bioceramic scaffolds. Proc Inst Mech Eng H. 2017;231(6):575–85.
[34] S. Bose, S. Vahabzadeh, and A. Bandyopadhyay, “Bone tissue engineering using 3D printing,” Mater. Today, vol. 16, no. 12, pp. 496–504, 2013.

[35] A. M. H. Ng et al., “Differential osteogenic activity of osteoprogenitor cells on HA and TCP/HA scaffold of tissue engineered bone,” J. Biomed. Mater. Res. - Part A, vol. 85, no. 2, pp. 301–312, 2008.
[36] D. W. Hutmacher, M. Sittinger, and M. V. Risbud, “Scaffold-based tissue engineering: Rationale for computer-aided design and solid free-form fabrication systems,” Trends Biotechnol., vol. 22, no. 7, pp. 354–362, 2004.
[37] J. O. Hollinger, T. A. Einhorn, B. A. Doll, and C. Sfeir, “Rapid prototyping technology and its application in bone tissue engineering,” J. Zhejiang Univ. B (Biomedicine Biotechnol., vol. 18, no. 4, pp. 303–315, 2017.
[38] M. Fantini, M. Curto, and F. De Crescenzio, “A method to design biomimetic scaffolds for bone tissue engineering based on Voronoi lattices,” Virtual Phys. Prototyp., vol. 11, no. 2, pp. 77–90, 2016.
[39] S. M. Giannitelli, D. Accoto, M. Trombetta, and A. Rainer, “Current trends in the design of scaffolds for computer-aided tissue engineering,” Acta Biomater., vol. 10, no. 2, pp. 580–594, 2014.
[40] C. Schmidleithner, “Master Thesis Additive Manufacturing of Tricalcium Phosphate Scaffolds for Bone Tissue Engineering,” Vienna University of Technology.
[41] F. Baino, J. Barberi, E. Fiume, G. Orlygsson, J. Massera, and E. Vern, “Robocasting of Bioactive SiO2-P2O5-CaO-MgO-Na2O-K2O Glass Scaffolds,” J. Healthc. Eng., vol. 2019, 2019.
[42] M. Moesen, T. Craeghs, J. P. Kruth, and J. Schrooten, “Robust beam compensation for laser-based additive manufacturing,” CAD Comput. Aided Des., vol. 43, no. 8, pp. 876–888, 2011.
[43] E. S. Bishop et al., “3-D bioprinting technologies in tissue engineering and regenerative medicine: Current and future trends,” Genes Dis., vol. 4, no. 4, pp. 185–195, 2017.
[44] A. D. Lantada, A. De Blas Romero, M. Schwentenwein, C. Jellinek, and J. Homa, “Lithography-based ceramic manufacture (LCM) of auxetic structures: Present capabilities and challenges,” Smart Mater. Struct., vol. 25, no. 5, 2016.
[45] C. Sun, N. Fang, D. M. Wu, and X. Zhang, “Projection micro-stereolithography using digital micro-mirror dynamic mask,” Sensors Actuators, A Phys., vol. 121, no. 1, pp. 113–120, 2005.
[46] Y. Mao, T. Miyazaki, K. Sakai, J. Gong, M. Zhu, and H. Ito, “A 3D printable thermal energy storage crystalline gel using mask-projection stereolithography,” Polymers (Basel)., vol. 10, no. 10, pp. 1–14, 2018.
[47] J. H. Lee, R. K. Prud’homme, and I. A. Aksay, “Cure depth in photopolymerization: Experiments and theory,” J. Mater. Res., vol. 16, no. 12, pp. 3536–3544, 2001.
[48] M. L. Griffith and J. W. Halloran, “Ultraviolet curable ceramic suspensions for stereolithography of ceramics,” Am. Soc. Mech. Eng. Prod. Eng. Div. PED, vol. 68–2, no. January 1994, pp. 529–534, 1994.
[49] C. J. Bae, A. Ramachandran, K. Chung, and S. Park, “Ceramic stereolithography: Additive manufacturing for 3D complex ceramic structures,” J. Korean Ceram. Soc., vol. 54, no. 6, pp. 470–477, 2017.
[50] A. de Blas Romero et al., “Lithography-based additive manufacture of ceramic biodevices with design-controlled surface topographies,” Int. J. Adv. Manuf. Technol., vol. 88, no. 5–8, pp. 1547–1555, 2017.

[51] S. P. Gentry and J. W. Halloran, “Depth and width of cured lines in photopolymerizable ceramic suspensions,” J. Eur. Ceram. Soc., vol. 33, no. 10, pp. 1981–1988, 2013.
[52] C. Hinczewski, S. Corbel, and T. Chartier, “Ceramic suspensions suitable for stereolithography,” J. Eur. Ceram. Soc., vol. 18, no. 6, pp. 583–590, 1998.
[53] J. Bennett, “Measuring UV curing parameters of commercial photopolymers used in additive manufacturing,” Addit. Manuf., vol. 18, pp. 203–212, 2017.
[54] F. Scalera, C. Esposito Corcione, F. Montagna, A. Sannino, and A. Maffezzoli, “Development and characterization of UV curable epoxy/hydroxyapatite suspensions for stereolithography applied to bone tissue engineering,” Ceram. Int., vol. 40, no. 10, pp. 15455–15462, 2014.
[55] T. Chartier, C. Chaput, F. Doreau, and M. Loiseau, “Stereolithography of structural complex ceramic parts,” J. Mater. Sci., vol. 37, no. 15, pp. 3141–3147, 2002.
[56] J. W. Halloran et al., “Photopolymerization of powder suspensions for shaping ceramics,” J. Eur. Ceram. Soc., vol. 31, no. 14, pp. 2613–2619, 2011.
[57] G. Mitteramskogler et al., “Light curing strategies for lithography-based additive manufacturing of customized ceramics,” Addit. Manuf., vol. 1, pp. 110–118, 2014.
[58] E. Schwarzer, M. Götz, D. Markova, D. Stafford, U. Scheithauer, and T. Moritz, “Lithography-based ceramic manufacturing (LCM) – Viscosity and cleaning as two quality influencing steps in the process chain of printing green parts,” J. Eur. Ceram. Soc., vol. 37, no. 16, pp. 5329–5338, 2017.
[59] C. Schmidleithner, S. Malferarri, R. Palgrave, D. Bomze, M. Schwentenwein, and D. M. Kalaskar, “Application of high resolution DLP stereolithography for fabrication of tricalcium phosphate scaffolds for bone regeneration,” Biomed. Mater., vol. 14, no. 4, pp. 1–11, 2019.
[60] Y. Zeng et al., “3D printing of hydroxyapatite scaffolds with good mechanical and biocompatible properties by digital light processing,” J. Mater. Sci., vol. 53, no. 9, pp. 6291–6301, 2018.
[61] R. Felzmann et al., “Lithography-based additive manufacturing of cellular ceramic structures,” Adv. Eng. Mater., vol. 14, no. 12, pp. 1052–1058, 2012.
[62] D. Ko, K. Gyak, D. Kim. “Emerging microreaction systems based on 3D printing techniques and aeparation technologies,” J. Flow Chem., vol. 7, pp. 72–81, 2017.
[63] Y. Lu, G. Mapili, G. Suhali, S. Chen, and K. Roy, “A digital micro-mirror device-based system for the microfabrication of complex, spatially patterned tissue engineering scaffolds,” J. Biomed. Mater. Res. - Part A, vol. 77, no. 2, pp. 396–405, 2006.
[64] L. H. Han, G. Mapili, S. Chen, and K. Roy, “Projection microfabrication of three-dimensional scaffolds for tissue engineering,” J. Manuf. Sci. Eng. Trans. ASME, vol. 130, no. 2, pp. 0210051–0210054, 2008.
[65] I. Potestio, “Lithoz: How lithography-based ceramic AM is expanding the opportunities for technical ceramics,” Powder Inject. Mould. Int., vol. 13, no. 2, pp. 2–5, 2019.
[66] C. Mangano, F. Mangano, L. Gobbi, O. Admakin, S. Iketani, and A. Giuliani, “Comparative study between laser light stereo-lithography 3D-printed and traditionally sintered biphasic calcium phosphate scaffolds by an integrated morphological, morphometric and mechanical analysis,” Int. J. Mol. Sci., vol. 20, no. 13, 2019.
[67] P. Tesavibul et al., “Biocompatibility of hydroxyapatite scaffolds processed by lithography-based additive manufacturing,” Biomed. Mater. Eng., vol. 26, no. 1–2, pp. 31–38, 2015.

[68] Y. Yao, N. Sha, and Z. Zhao, “Highly Concentrated Hydroxyapatite Suspension for DLP Printing,” IOP Conf. Ser. Mater. Sci. Eng., vol. 678, no. 1, pp. 1–8, 2019.
[69] P. Tesavibul et al., “Processing of 45S5 Bioglass® by lithography-based additive manufacturing,” Mater. Lett., vol. 74, pp. 81–84, 2012.
[70] C. Ghayor and F. E. Weber, “Osteoconductive microarchitecture of bone substitutes for bone regeneration revisited,” Front. Physiol, vol. 9, pp. 1–10, 2018.
[71] Z. Liu et al., “Additive manufacturing of hydroxyapatite bone scaffolds via digital light processing and in vitro compatibility,” Ceram. Int., vol. 45, no. 8, pp. 11079–11086, 2019.
[72] C. Feng et al., “Additive manufacturing of hydroxyapatite bioceramic scaffolds: Dispersion, digital light processing, sintering, mechanical properties, and biocompatibility,” J. Adv. Ceram., vol. 9, no. 3, pp. 360–373, 2020.
[73] Y. Cao et al., “Fabrication and properties of zirconia/hydroxyapatite composite scaffold based on digital light processing,” Ceram. Int., vol. 46, no. 2, pp. 2300–2308, 2020.